Supplementary Information

Table of Contents

Supplementary Table 1: VAAT lesion sizes in swine where experimental mapping-based ablation failed to terminate VT.

Swine	Ablation size (cm^3)
3	0.15
4	2.25
5	0.13

Supplementary Table 2: VAAT total volume of the ablation lesions in the retrospective human study (n = 16).

Patient	Ablation size (cm^3)
1	0.10
2	0.22
3	0.10
4	0.72
5	0.52
6	0.71
7	0.53
8	0.56
9	2.52
10	0.16
11	2.00
12	0.64
13	1.98
14	1.57
15	1.56
16	2.61

Supplementary Table 3: Myocardial wall artifact burdens and VAAT lesion sizes in the retrospective human study involving patients with ICDs (n = 5).

Patient	Artifact Burden	Ablation size (cm^3)
1	59%	0.31
2	46%	0.36
3	1%	0.68
4	0%	0.79
5	62%	0.17

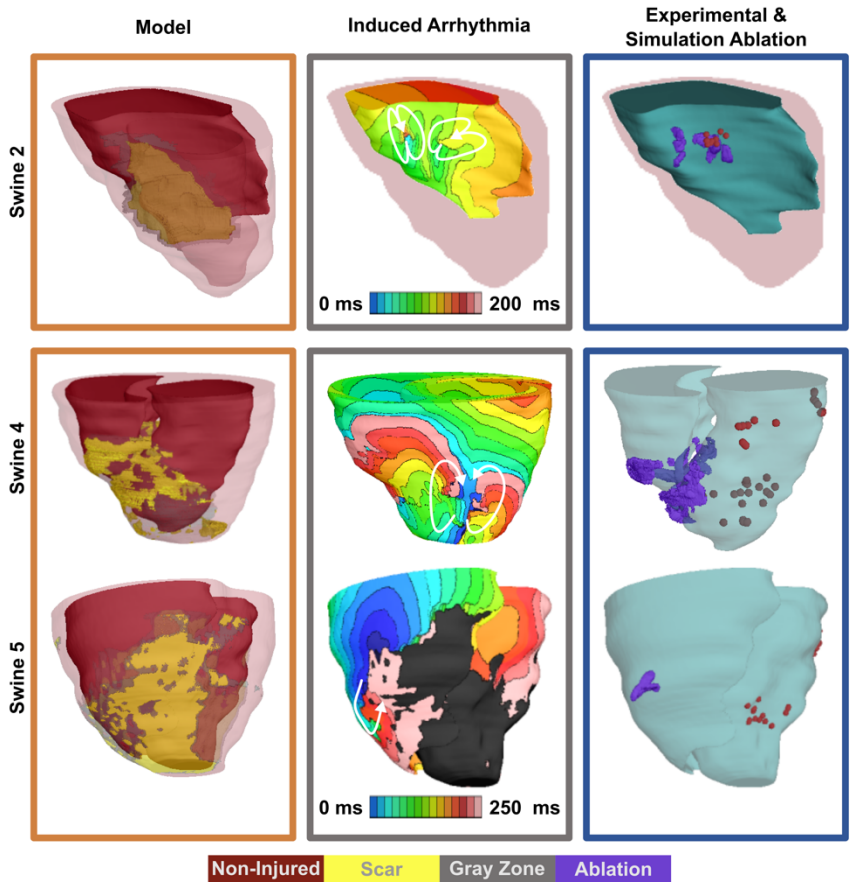

Supplementary Figure 1: *VAAT prediction: results from the remaining 3 swine hearts in the animal study*. Illustrated are one case of successful (Swine 2) and two cases of failed (Swine 4 and 5) mapping-guided ablation and the respective models and VAAT predictions. Image frame colors correspond to the steps outlined in Fg.1A. Panels present, from left to right: reconstructed ventricular models with different remodeled regions; endocardial (Swine 2) or epicardial (Swine 4 and 5) electrical activation maps of the infarct-related VTs and arrows showing direction of propagation; VAAT predicted ablation targets (purple) on the ventricular endocardial (Swine 2) or epicardial (Swine 4 and 5) surface; and comparison of these with experimental mapping-based endocardial ablation locations. In the latter images, red dots represent locations of the tip of the catheter during ablation; to depict those, ventricular geometry from post-ablation CT scans was co-registered with the MRI-based model. Note that in Swine 2, VAAT predicted that two VT reentrant circuits could be sustained by the ventricular substrate. Only one of these was manifested in the animal during the procedure, and the corresponding target ablated. Identifying all possible VT circuits that can be sustained in a given substrate, and not only those manifested or induced at the time of procedure is an advantage of our approach since it could decrease or even eliminate the need for repeated ablations.

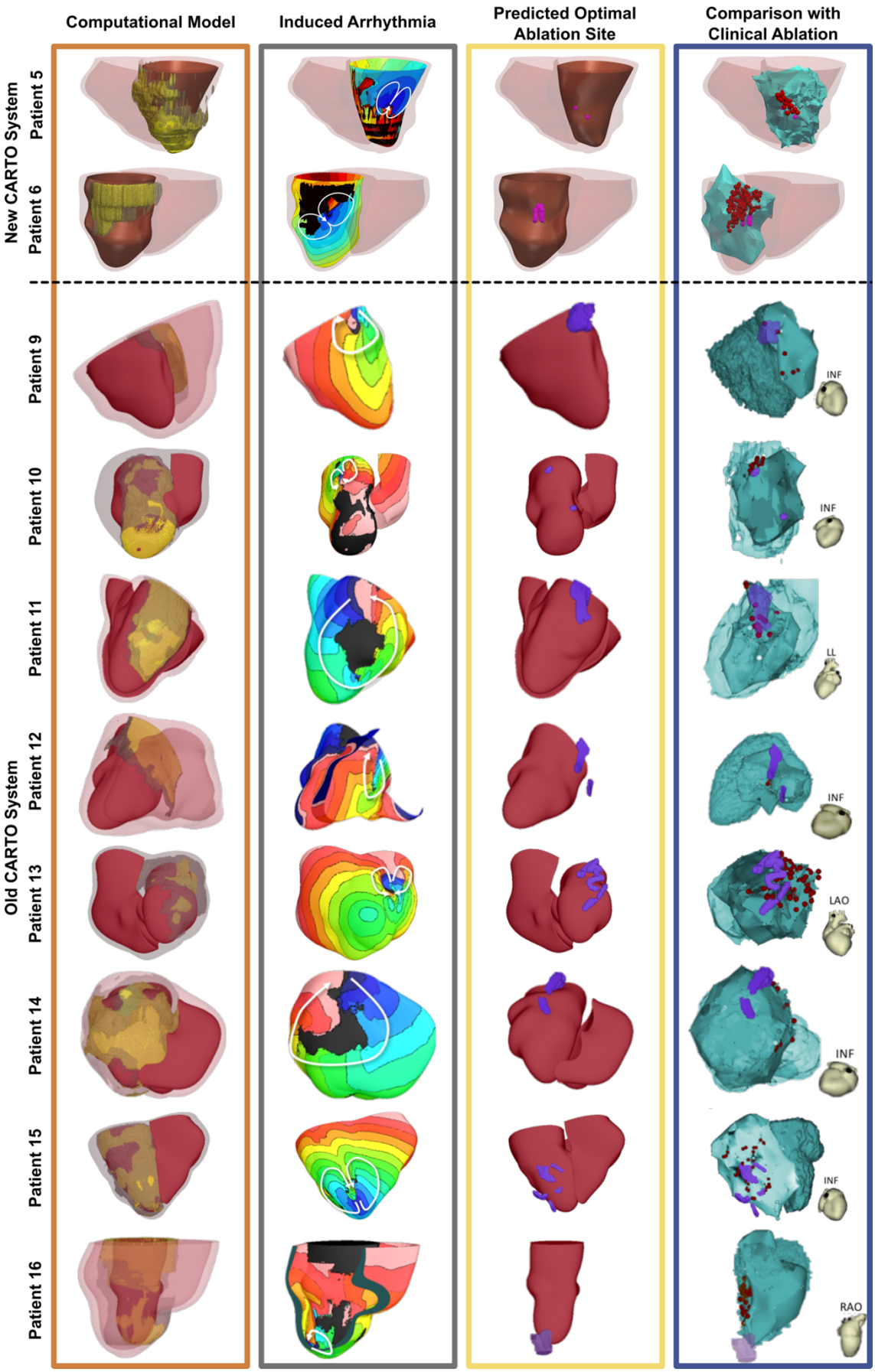
Computational Model
Induced Arrhythmia
Predicted Optimal Ablation Site
Comparison with Clinical Ablation
New CARTO System
Patient 5
Patient 6
Old CARTO System
Patient 9
Patient 10
Patient 11
Patient 12
Patient 13
Patient 14
Patient 15
Patient 16
INF
INF
LL
INF
LAO
INF
INF
RAO

Supplementary Figure 2 (previous page): *Results from additional 10 patient heart models in the retrospective human study*. Image frame colors correspond to the steps outlined in Fg.1A. The top 2 patients were ablated using a newer version of the CARTO electroanatomical navigation system, the same used for the results shown in Fig. 2. The remaining 8 patients were ablated using an older version of the CARTO system. Panels present, from left to right: reconstructed ventricular models with different structurally-remodeled regions; electrical activation maps of the infarct-related VTs on the epi- or endocardial surfaces (chosen for best visualization) and arrows showing direction of propagation; VAAT predicted ablation targets (purple) on the endocardial surface; and co-registration of the VAAT targets with the CARTO endocardial surface (green) showing clinical ablation locations (red dots represent locations of the tip of the catheter during ablation). Small hearts at bottom left show heart orientation in the older CARTO system (LAO = left anterior oblique, RAO = right anterior oblique, and INF = inferior view).

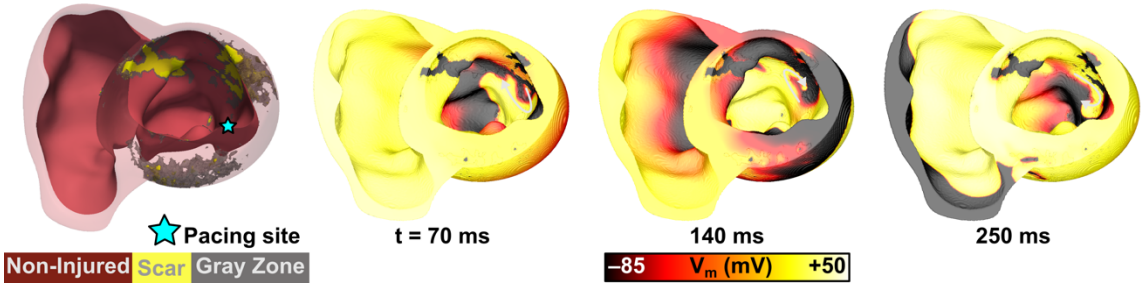

Supplementary Figure 3: *Initiation of sustained VT in the heart model of the patient from the prospective human study at the University of Utah (corresponding to one of the VT morphologies in Fig. 3a).* Shown are patient heart geometry and transmembrane potential maps of one of the induced VTs in this patient at three time instants. White arrows show direction of propagation. Time below each map is counted from the delivery of the last pacing stimulus. Propagation through a channel in the scar is visible. See also Supplementary Movie 2.

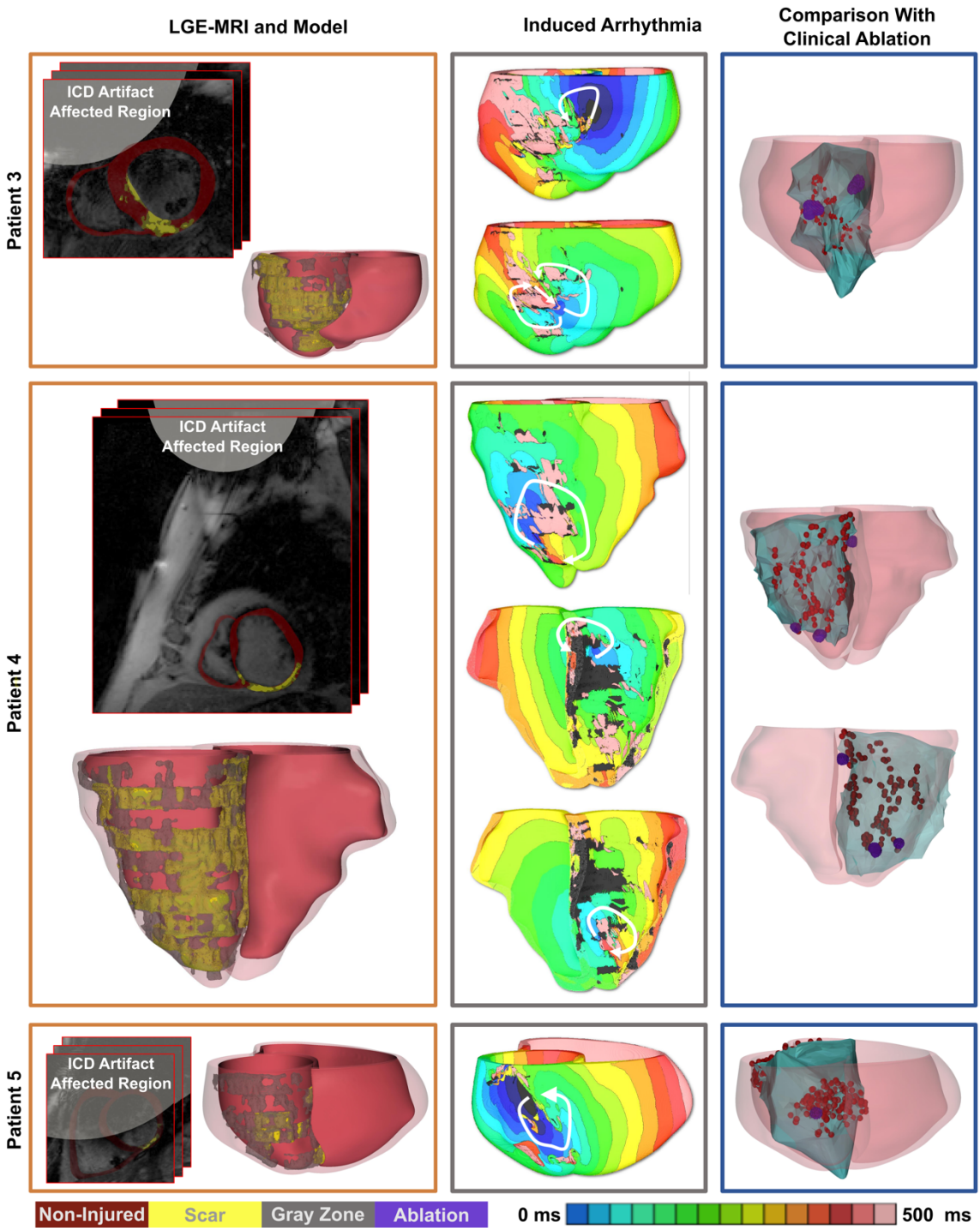

Supplementary Figure 4: *Results from the remaining 3 human heart models in the retrospective study in patients with ICDs.* Panel frame colors corresponds to Fig.1a. Panels present, from left to right: LGE-MRI scans with ICD artifact burden and reconstructed ventricular models with different remodeled regions; electrical

activation maps of the infarct-related VTs on the epicardial surfaces and arrows showing direction of VT propagation; and co-registration of ventricular model surfaces and VAAT-predicted ablation targets with the CARTO endocardial surface (green) showing clinical ablation locations (red dots representing locations of the tip of the catheter during ablation). In patients 3 and 4, the ICD artifact did not cover the myocardial wall. In patient 5, the ICD artifact covered 62% of the myocardial wall. In all cases, VAAT-predicted targets were located within the areas ablated clinically. In Patient 5, there was an additional clinical ablation on the anterior LV wall that was not predicted by the simulations since that part of the ventricular wall was covered by the ICD artifact. In such severe cases, non-invasive ablation target prediction can only partially substitute electrical mapping. We expect that in such cases, in the clinical implementation the predicted targets will be first ablated, and if VT remains inducible, then mapping can be used to determine the remaining ablation target(s) that the simulations could not reveal.

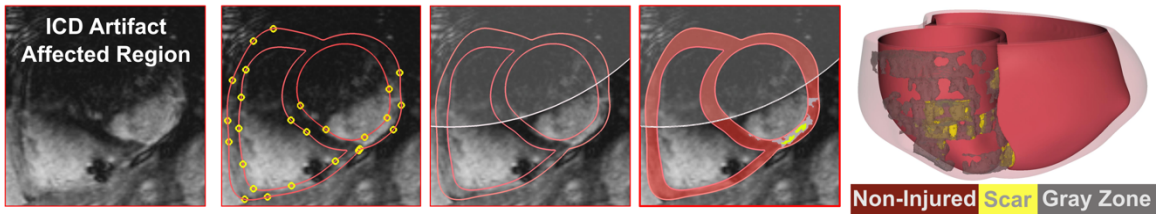

Supplementary Figure 5: *Ventricular model construction from LGE MRI scans with ICD artifact burden.* Panels present, from left to right: LGE MRI scans with ICD artifact burden; ventricular myocardial wall segmentation relying on the prominent boundaries of the visible myocardial wall and extrapolation into areas covered by the artifact; delineation of ICD artifact in the ventricular myocardium based on the 3D radial distance from the ICD; myocardial tissue classification; and resulting ventricular model.

Supplementary Movie 1: Initiation of VT for patient 2 in the retrospective human study of patients with ICDs. The movie starts at 300 ms after the delivery of the sixth S1 (t = 2550 ms) and shows the subsequent delivery of S2 (t = 2570 ms) and S3 (t = 2800 ms), and then 2000-ms period of induced VT. Note wavefront propagation through patchy infarct areas.

Supplementary Movie 2: Initiation of sustained VT in the heart model of the patient from the prospective human study at the University of Utah (corresponding to one of the VT morphologies in Fig. 3a, and to Supplementary Figure 3).